

Bumblebee cosmology: Tests using distance- and time-redshift probes

XINCHENG ZHU,¹ RUI XU,¹ AND DANDAN XU¹

¹*Department of Astronomy, Tsinghua University, Beijing 100084, People's Republic of China;*

ABSTRACT

In modern cosmology, the discovery of the universe's accelerated expansion has significantly transformed our understanding of cosmic evolution and expansion history. The unknown properties of dark energy, the driver of this acceleration, have not only prompted extensive studies on its nature but also spurred interest in modified gravity theories that might serve as alternatives. In this paper, we adopt a bumblebee vector-tensor modified gravity theory to model the cosmic expansion history and derive predictions for the Hubble parameter. We constrain the bumblebee model parameters using observational data from established probes, including the Pantheon+ SH0ES Type Ia Supernovae and BAO measurements from DESI DR1, as well as recently included Cosmic Chronometers and Gamma Ray Bursts data. The Markov Chain Monte Carlo sampling of Bayesian posterior distribution enables us to rigorously constrain the bumblebee model and compare it with the standard Λ CDM cosmology. Our results indicate that the bumblebee theory provides a compatible fit with current observational data across a range of its parameters, suggesting it as a viable alternative to the Λ CDM model.

1. INTRODUCTION

The standard cosmological model in general relativity (GR) requires dark energy to account for the currently observed accelerated expansion of the universe (Riess et al. 1998; Copeland et al. 2006). As the substance of dark energy is mysterious, dynamical fields are popular substitutions of dark energy (Akrami et al. 2021). Abundant research on substituting dark energy using scalar fields has been done in the literature (for reviews see, e.g., Copeland et al. (2006); Bamba et al. (2012); Ji & Shao (2024)). We investigate substituting dark energy using a vector field that nonminimally couples to the Ricci curvature tensor and to the Ricci curvature scalar. The theory is called the bumblebee gravitational theory (Kostelecký 2004), and its action is

$$S = \frac{1}{16\pi} \int d^4x \sqrt{-g} (R + \xi_1 B^\mu B^\nu R_{\mu\nu} + \xi_2 B^\mu B_\mu R) - \int d^4x \sqrt{-g} \left(\frac{1}{4} B^{\mu\nu} B_{\mu\nu} + V \right), \quad (1)$$

where the geometrized unit system, $G = c = 1$, has been used, and g is the determinant of the spacetime metric $g_{\mu\nu}$. The bumblebee theory is a vector-tensor theory of gravity where the vector field B_μ modifies the

behavior of gravity not only through the kinetic term $B^{\mu\nu} B_{\mu\nu}$ and the potential term V , but also through the coupling terms $B^\mu B^\nu R_{\mu\nu}$ and $B^\mu B_\mu R$. Note that the field strength $B_{\mu\nu}$ is defined in the same way as the field strength of the electromagnetic field, namely

$$B_{\mu\nu} = \partial_\mu B_\nu - \partial_\nu B_\mu. \quad (2)$$

The two coupling constants ξ_1 and ξ_2 control the sizes of the nonminimal couplings.

Hellings and Nordtvedt first studied the theory in Eq. (1) but without the potential term V (Hellings & Nordtvedt 1973). Then, this theory was reintroduced by Kostelecký with the potential term V to study possible breaking of Lorentz symmetry in curved spacetime (Kostelecký 2004). To generate a vacuum expectation value for the vector field B_μ that breaks Lorentz symmetry, the potential V is commonly assumed to be minimized at some nonzero configuration of B_μ (Kostelecký 2004; Bluhm & Kostelecký 2005; Bailey & Kostelecký 2006), putting up the chance of connecting dark energy to Lorentz-symmetry violation. In this work, we intend not to dwell on the Lorentz-symmetry violating aspect of the bumblebee theory, but focus on the simplest form of the potential,

$$V = V_1 B^\mu B_\mu, \quad (3)$$

where V_1 is a constant. A rather interesting Friedmann-Lemaître-Robertson-Walker (FLRW) metric solution

has been found in the bumblebee theory with this potential in Xu et al. (in preparation), generalizing the FLRW solution found by Hellings and Nordtvedt (Hellings & Nordtvedt 1973). The aim of this work is to give a thorough examination of the cosmological solution using modern astronomical observations of cosmic distances and time as functions of redshift.

The derivation and a detailed account of the FLRW solution in the bumblebee theory with the potential in Eq. (3) is presented in Xu et al. (in preparation). Here we directly write down the solution for our use. It is

$$\begin{aligned} \frac{H(z)}{H_0} &:= E(z) \\ &= \sqrt{\Omega_{V_1} + (1 - \Omega_{V_1} - \Omega_{\mathcal{K}0})(1+z)^{2-\alpha} + \Omega_{\mathcal{K}0}(1+z)^2}, \end{aligned} \quad (4)$$

where $H(z)$ is the Hubble variable as a function of the redshift z , H_0 is the Hubble constant, and $\Omega_{\mathcal{K}0}$ represents the current fractional density parameter corresponding to the spatial curvature of the universe. The new parameters Ω_{V_1} and α are related to the coupling constants ξ_1 , ξ_2 and the potential parameter V_1 via

$$\begin{aligned} \Omega_{V_1} &= \frac{2\tilde{V}_1}{\xi_1 + 4\xi_2}, \\ \alpha &= -\frac{4\xi_2}{\xi_1 + 2\xi_2}, \end{aligned} \quad (5)$$

with $\tilde{V}_1 = 8\pi V_1 / (3H_0^2)$. The solution is unconventional because the role played by the densities of matter and radiation in the conventional Λ CDM solution is replaced by the $(1+z)^{2-\alpha}$ term, which is a consequence of the nonminimal couplings in Eq. (1), resulting in an expansion rate of the universe completely independent of the matter and radiation in it. We also point out that the role of the dark energy in the conventional Λ CDM solution is now replaced by Ω_{V_1} , which is proportional to the potential parameter V_1 , i.e. the square of the mass of the vector field.

To investigate whether this unconventional solution offers a workable alternative to explain the universe's late-time acceleration, various cosmological distances and time calculated using the expansion rate in Eq. (4), as functions of the redshift z , will be tested against observational data sets from Type Ia supernovae (SNe Ia) (Brout et al. 2022), baryon acoustic oscillations (BAO) (DESI Collaboration et al. 2024a), cosmic chronometers (CC) (Stern et al. 2010; Moresco et al. 2016), and long gamma-ray bursts (GRB) (Moresco et al. 2022). In Section 2, we summarize the information of data and the structure of our Bayesian posterior inference for pa-

rameter constraints; in Section 3, we present the posterior inference results and compare them with the result from the conventional Λ CDM model; and in Section 4, we make concluding remarks. The resultant constraints will be presented in terms of the parameters H_0 , $\Omega_{\mathcal{K}0}$, α , and $\tilde{\xi}_1 := \xi_1/\tilde{V}_1$.

2. DATA AND ANALYSIS

In this work, we use the observational data mentioned above to constrain the bumblebee model parameters. We use the Markov Chain Monte Carlo (MCMC) to sample the posterior distributions which are determined by both the prior information and the likelihood function. In this study, we use a Gaussian likelihood function, which incorporates a pseudo chi-squared function. The likelihood is given by:

$$\mathcal{L} \propto \exp(-\chi^2/2), \quad \chi^2 = \sum_i \frac{(y_i - y_{\text{model},i})^2}{\sigma_i^2} \quad (6)$$

where χ^2 is the pseudo chi-squared function, y_i represents the observational data, $y_{\text{model},i}$ is the model prediction by cosmological model, and σ_i denotes the uncertainties including potential systematic errors in the observational data.

2.1. Pantheon+ SH0ES Type Ia Supernovae

Type Ia supernovae (SNe Ia) are widely used as standard candles to measure the cosmic expansion history. The luminosity distance of SNe Ia at different redshifts can be inferred using their apparent magnitudes and redshifts, given a specific cosmological model.

In this analysis, we adopt the largest SNe Ia sample published to date, the Pantheon+ compilation (Brout et al. 2022). It is an extended compilation of the original Pantheon analysis (Scolnic et al. 2018) with 1701 SNe Ia light curves from 18 different surveys, covering a redshift range from 0.001 to 2.26. As the successor to the original Pantheon analysis, this dataset provides a more comprehensive collection of supernovae. It also includes supernovae that are in galaxies with measured Cepheid host distances and covariance (SH0ES), allowing for simultaneous constraints on parameters that describe the full expansion history of the universe. The chi-square function is defined as:

$$\chi_{\text{SN}}^2 = \sum_{i=1}^{1701} \frac{(\mu_{\text{obs},i} - \mu_{\text{th},i})^2}{\sigma_{\text{obs},i}^2}, \quad (7)$$

where $\mu_{\text{obs},i}$ is the observed distance modulus and $\sigma_{\text{obs},i}$ is the corresponding uncertainty in the observed distance modulus. The theoretical distance modulus $\mu_{\text{th},i}$ is defined as $\mu_{\text{th},i}(z) = m - M = 5 \log_{10} \left(\frac{D_{\text{lum}}(z)}{\text{Mpc}} \right) + 25$,

where D_{lum} is the luminosity distance, which is given by $D_{\text{lum}}(z) = \frac{c(1+z)}{H_0} \int_0^z \frac{dz'}{E(z')}$.

2.2. BAO measurements from DESI DR1 galaxy spectral survey

Baryon Acoustic Oscillations (BAO) trace the comoving size of the sound horizon r_d at the drag reshift $z_d \approx 1100$ when baryons were released from photons. The BAO clustering signal can be used to measure the angular diameter distance $D_A(z)$ and the Hubble parameter $H(z)$ at different redshifts.

We use the BAO measurements from the Dark Energy Spectroscopic Instrument (DESI) Data Release 1 (DR1) (DESI Collaboration et al. 2024a). DESI is the most updated and advanced Stage IV galaxy survey project. The DESI DR1 features a massive dataset comprising over 5.7 million unique galaxy and quasar redshifts in the range $0.1 < z < 2.1$, enabling high-precision BAO measurements with a sophisticated blinding technique to minimize confirmation bias (DESI Collaboration et al. 2024b). The relation between BAO measurements and the cosmic expansion history are given by the angular diameter distance (transverse signal) and Hubble parameter (line-of-sight signal) at different redshifts. The chi-square function is defined as:

$$\chi_{\text{BAO}}^2 = \sum_{i=1}^7 \frac{\left((D_V/r_d)_{\text{obs},i} - (D_V/r_d)_{\text{th},i} \right)^2}{\sigma_{\text{obs},i}^2}, \quad (8)$$

where D_V/r_d is the ratio of the angle-averaged distance D_V to the sound horizon scale r_d , which is given by $D_V(z) = (z(1+z)^2 D_A^2(z) D_H(z))^{1/3}$, with $D_A(z)$ and $D_H(z)$ being the angular diameter distance and the Hubble distance, respectively.

2.3. Cosmic Chronometers (CC)

Cosmic Chronometers (CC), as the new emerging probes, are a class of galaxies that are passively evolving and have a well-defined star formation history. The age of these galaxies can be inferred from their stellar populations, which can be used to measure the cosmic expansion history. The Hubble parameter $H(z)$ can be inferred from the differential age of the universe $t(z)$ at different redshifts (see Stern et al. 2010; Moresco et al. 2016).

The complete list of the sample we used is collectively presented in Tabel 1.1 of Moresco (2023). The chi-square function is defined as:

$$\chi_{\text{CC}}^2 = \sum_{i=1}^{35} \frac{(H_{\text{obs},i} - H_{\text{th},i})^2}{\sigma_{\text{obs},i}^2}, \quad (9)$$

where $H_{\text{obs},i}$ is the observed Hubble parameter derived from $H(z) = \frac{1}{1+z} \left(\frac{dz}{dt} \right)_{\text{obs}}$, and $\sigma_{\text{obs},i}$ is the corresponding uncertainty in the observed Hubble parameter.

2.4. (Long) Gamma Ray Bursts

Gamma-Ray Bursts (GRB) are the most energetic explosions in the universe that can reach up to $10^{48} - 10^{53}$ ergs in a few seconds. Bright GRBs can be detected up to redshifts of 10 (Moresco et al. 2022), while the most distant detectable SN Ia is only about redshift 2.5 for now. Several correlations have been found to make GRBs (especially long bursts) as quasistandard candles (Table 4 of Moresco et al. (2022)). The most investigated one is the Amati relation (Amati et al. 2002), which is an empirical correlation between the peak energy of the γ -ray spectrum and the isotropic equivalent energy of the burst.

The details of GRB samples we used can be found in Huang et al. (2021) and the redshift range of this data set is from 0.0331 to 8.1. The chi-square function is defined as:

$$\chi_{\text{GRB}}^2 = \sum_{i=1}^{179} \frac{(y_{\text{obs},i} - (kx_{\text{obs},i} + b))^2}{\sigma_{\text{obs},i}^2}, \quad (10)$$

where $y := \log_{10} \frac{E_{\text{iso}}}{\text{erg}}$, $x := \log_{10} \frac{E_p}{300\text{keV}}$, E_p is the observed rest-frame spectral peak energy, $E_{\text{iso}} = \frac{4\pi D_{\text{lum}}^2 S_{\text{bolo}}}{1+z}$ is the observed bolometric isotropic-equivalent radiated energy which is converted from the observable bolometric fluence S_{bolo} . k and b are two linear parameters which are called Amati coefficients. Since there may exist uncounted extra variabilities in this relation, we added an extra error term σ_{int} as Reichart et al. (2001) to the total uncertainty $\sigma_{\text{obs},i}^2 = \sigma_{\text{int}}^2 + \sigma_y^2 + b^2 \sigma_x^2$.

2.5. Joint Analysis

Finally, we combine the likelihoods of the data into two groups: the first group includes the Pantheon+ SNe Ia data and the DESI DR1 BAO data, representing the most powerful standard cosmological probes. The other group includes all four probes, including new emerging cosmological probes, i.e., CC and GRB. As a result, the relevant joint chi-square function is given by:

$$\begin{aligned} \chi_{\text{joint,g1}}^2 &= \chi_{\text{SN}}^2 + \chi_{\text{BAO}}^2 \\ \chi_{\text{joint,g2}}^2 &= \chi_{\text{SN}}^2 + \chi_{\text{BAO}}^2 + \chi_{\text{CC}}^2 + \chi_{\text{GRB}}^2 \end{aligned} \quad (11)$$

2.6. Posteriors Inference

We adopt flat priors for the bumblebee model parameters: $H_0 \in [50, 100]$, $\xi_1 \in [0, 2]$, $\alpha \in [-10, 2]$, and $\Omega_{\mathcal{K}0} \in [-1, 1]$. Using the Python package `emcee`

(Foreman-Mackey et al. 2013), we sample the posterior distributions with 200k steps. The corresponding corner plot for posterior distribution of individual probes are provided in Figure 1. Figure 2 shows the corner plot of the joint constraints in two groups: traditional high-precision probes (SNe Ia and BAO) and all probes, including emerging ones (SNe Ia and BAO plus CC and GRB).

The marginalized constraints on the bumblebee parameters are summarized in Table 1. Figure 3 presents the best-fit predictions (maximum a posteriori (MAP) point of the joint posterior distribution for four probes) of each probes from the bumblebee model. All results are compared to the Λ CDM model obtained using the same methodology.

2.7. Information Criteria

In this subsection, we compare the bumblebee model (curved or flat) and with the standard Λ CDM model using the Akaike Information Criterion (AIC) and the Bayesian Information Criterion (BIC). They are statistical tools used for model selection, balancing model fit and complexity. Introduced by Akaike (1974), AIC is defined as:

$$\text{AIC} = 2k + \frac{2k(k+1)}{N_{\text{tot}} - k - 1} - 2 \ln(\mathcal{L}_{\text{max}}), \quad (12)$$

Developed by Schwarz (1978), BIC also evaluates model quality but incorporates a stronger penalty for model complexity. It is calculated as:

$$\text{BIC} = k \ln(N_{\text{tot}}) - 2 \ln(\mathcal{L}_{\text{max}}), \quad (13)$$

Both AIC and BIC assess model fit while penalizing complexity, but they differ in their penalty strength. AIC applies a constant penalty per parameter, whereas BIC's penalty grows with sample size. Consequently, AIC tends to favor more complex models, especially with larger data sets, while BIC prefers simpler models as sample size increases. From the perspective of identifying the true model, BIC appears advantageous (Yang 2005). Both information criteria have their merits and limitations depending on the context. In most cases, the two will agree on the preferred model. When they diverge, the discrepancy itself provides valuable insights into the trade-offs between model fit and complexity. Here below we report both results for this work. Here we have 3 models to compare: Λ CDM, the spatially flat bumblebee model, and the spatially curved bumblebee model. The AIC and BIC values for each model are shown in Table 2 calculated by the best-fit parameters

of joint all 4 probes. The ΔIC ($\Delta\text{AIC}/\Delta\text{BIC}$) values are calculated by subtracting the minimum AIC or BIC values of the three, respectively. According to Jeffrey's scale (Kass & Raftery 1995), the condition $\Delta\text{IC} < 2$ confirms the statistical compatibility of the two models, and the model most favored by the data among this model set. A range of $2 < \Delta\text{IC} < 6$ suggests mild tension, while $\Delta\text{IC} \geq 10$ implies strong disagreement between the models.

3. DISCUSSION

3.1. Constraints on model parameters

As shown in Figures 1 and 2, the four probes are well-consistent for both flat and curved bumblebee models. The overlapping regions of the 2σ posterior distributions for individual probes align with the central 2σ region of the joint distribution, indicating no statistical tension between the probes. This consistency is further supported by the best-fit curves in Figure 3, where the jointly constrained parameters provide a good fit for all four probes. The corresponding minimum χ^2 values presented in Table 2 are comparable between the joint constraint and the sum of individual probe fits, confirming the self-consistency of the joint analysis.

Comparing the results using only traditional high-precision probes (SNe Ia and BAO) with those incorporating the emerging probes CC and GRB, we observe a slight shift in the center of the posterior distribution and a moderate narrowing of the constraints, particularly along the parameter degeneracy directions. The limited impact of the emerging probes can be attributed to two factors. First, as shown in Figure 1, the posterior distribution of CC is similar in shape to that of SNe Ia, albeit with a wider range due to larger systematic errors. The relatively larger errors and fewer data points compared to SNe Ia result in a smaller contribution to the total χ^2 . Second, GRB measurements suffer from significant uncertainties. While the Amati relation suggests a well-aligned linear relationship, the large intrinsic dispersion, substantial measurement errors, and the small sample size (179 GRBs) greatly weaken the constraining power of GRB as a probe (Figure 1). Although these two new probes contribute only marginally to the results, we argue that combining multiple probes is still of great significance. On one hand, emerging probes offer independent consistency checks, which can test the internal coherence of gravity models. On the other hand, with continuous advancements in observational techniques, the precision of these probes is expected to improve significantly in the foreseeable future

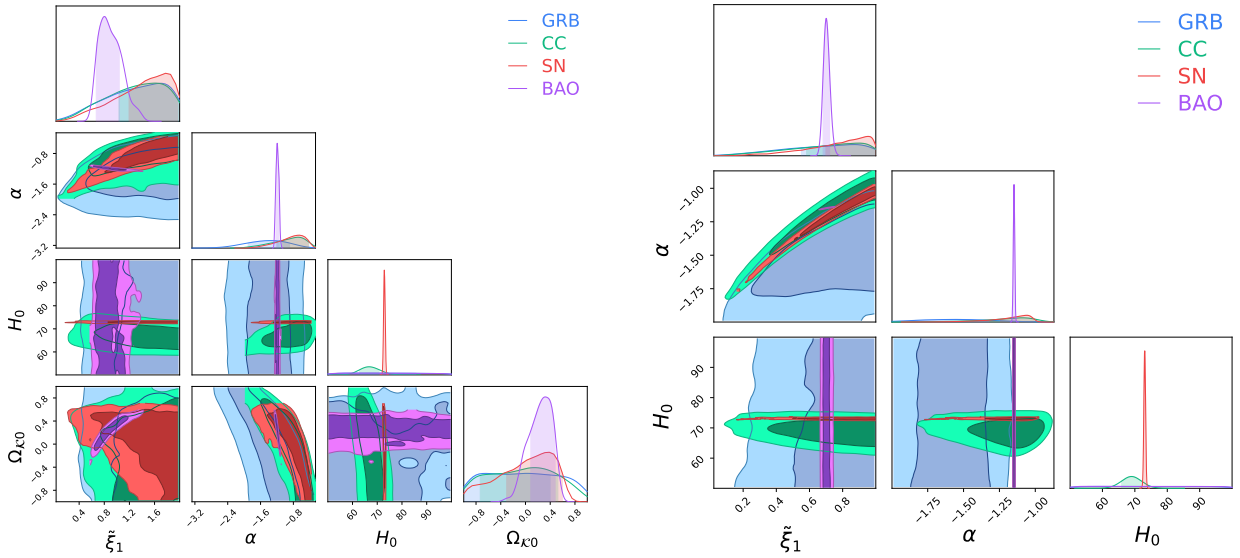


Figure 1. MCMC posterior distributions of 4 individual probes (SN, BAO, CC and GRB) for the spatially curved (left panel) and flat bumblebee models (right panel). The contours represent the 68% and 95% confidence levels.

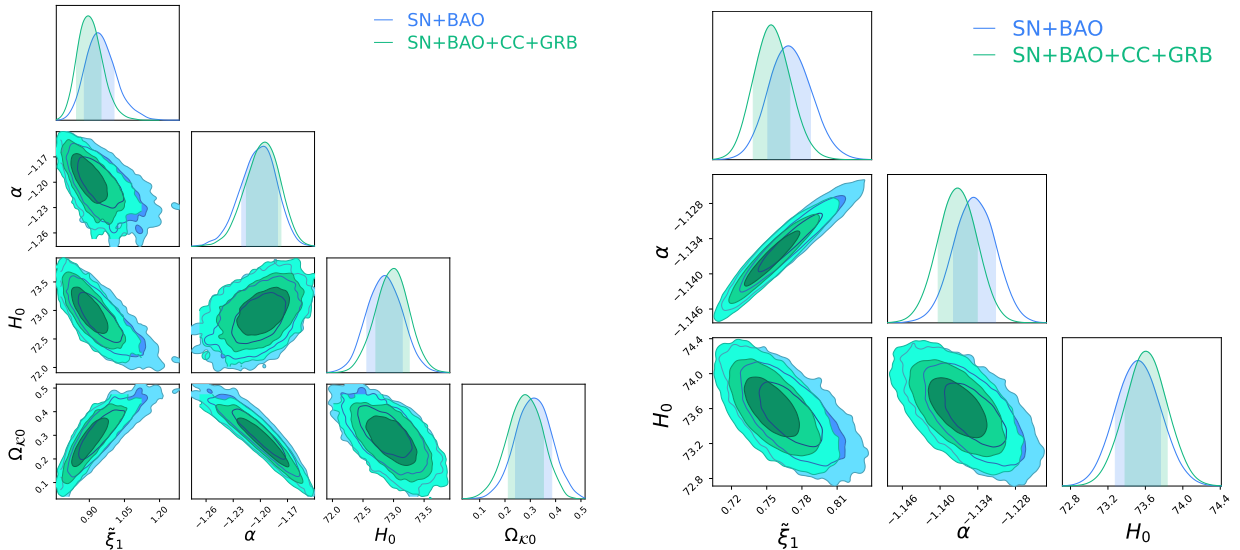


Figure 2. MCMC posterior distributions of the parameters for the spatially curved bumblebee model (left panel) and the spatially flat bumblebee model (right panel) from the joint analysis of Pantheon+ SH0ES SNe Ia, DESI DR1 BAO, CC, and GRB data. The contours represent the 68%, 95% and 99.7% confidence levels.

(Moresco et al. 2022). Over time, their advantages will become more evident: CC provides differential measurements that are independent of absolute values, and GRB probes span a wider redshift range and are less affected by dust or gas absorption. Therefore, we believe our approach is forward-looking and holds great promise.

The results from curved bumblebee model favor an open universe with a curvature parameter $\Omega_{\mathcal{K}0} \sim 0.3$. To date, no direct evidence suggests a non-trivial topology for our universe. While standard inflation predicts $\Omega_0 = 1$, modified inflationary scenarios like “open inflation” allow for $\Omega_0 < 1$ or $\Omega_0 > 1$. In the open infla-

tion model, a significantly sub-unity density parameter is naturally explained, supporting the possibility of a non-flat universe (Bucher & Turok 1995; Linde 1998).

The results suggest that Ω_{V_1} dominates at approximately 55%, followed by $\Omega_{\mathcal{K}0} \sim 29\%$ in the curved model. In contrast, the flat bumblebee model estimates $\Omega_{V_1} \approx 73\%$. Comparing to the Λ CDM model, the bumblebee parameter Ω_{V_1} can be interpreted as the equivalent of dark energy. The curved bumblebee model constrains the evolution index $(2 - \alpha)$ for $1 - \Omega_{V_1} - \Omega_{\mathcal{K}0}$ (see Eq. (4)) to 3.2, with the BAO probe providing the strongest constraint due to its dependence on the sound

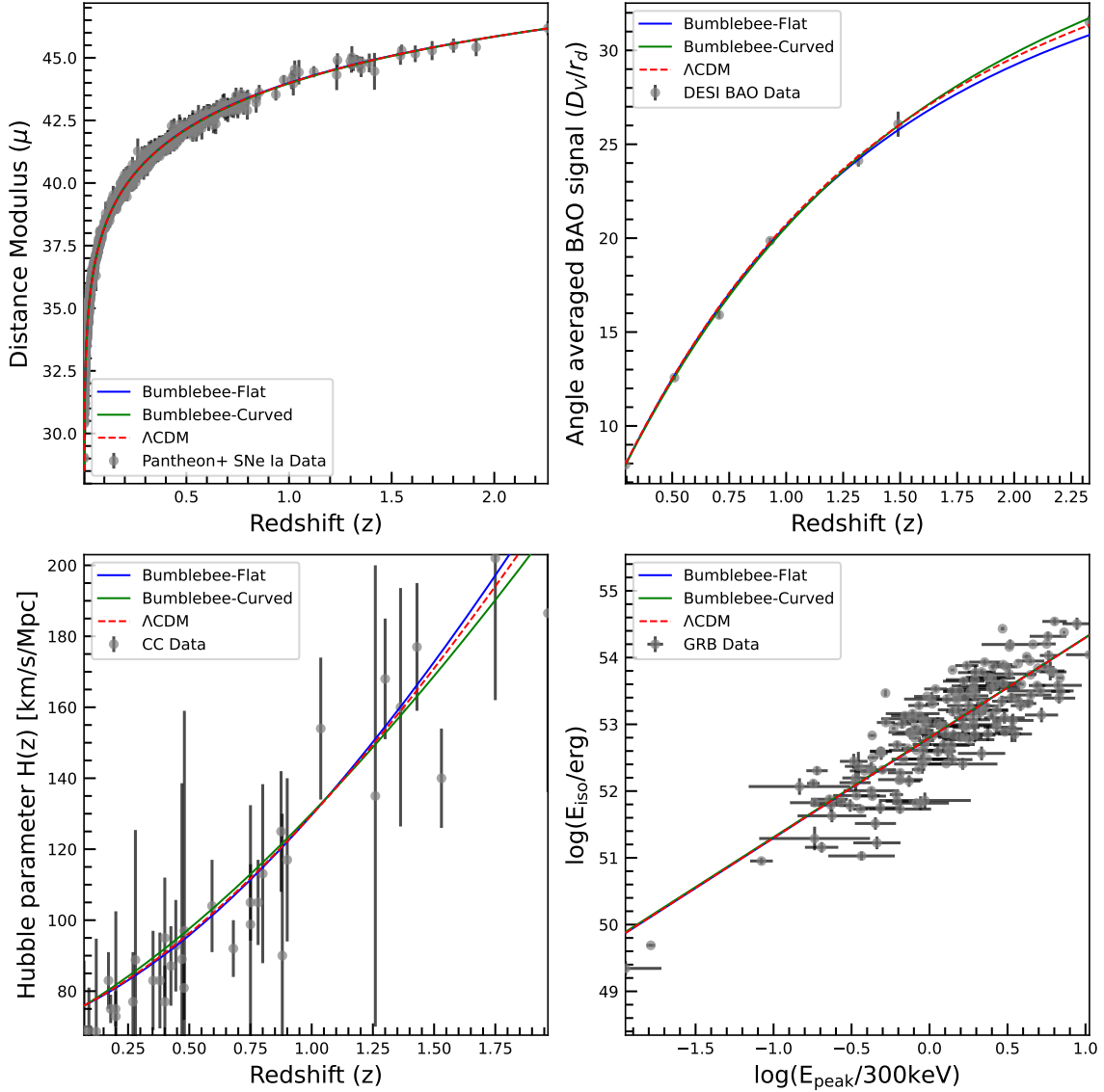


Figure 3. The best fit prediction (MAP) of 4 observational probes for the spatially curved bumblebee model and the spatially flat bumblebee model compared with the standard Λ CDM model.

horizon scale r_d . While the flat bumblebee model gives a slightly smaller power index of 3.14.

3.2. Model comparison: Bumblebee vs. Λ CDM

From Table 2, the χ^2 and reduced- χ^2 values for the two bumblebee models are comparable to those of the Λ CDM model, with no statistically significant differences. When penalizing for model complexity, the Δ AIC values (AIC and BIC) provide further insights. Using each of the four data sets as individual probes, Λ CDM consistently outperforms the bumblebee models. This is because the bumblebee models do not achieve significantly better χ^2 fits, yet involve more parameters (the Λ CDM model here assumes flatness and ignored radiation). Both Δ AIC and Δ BIC values for bumblebee

models compared to Λ CDM fall between mild tension and strong disagreement.

For joint constraints, the situation changes if using Δ AIC for model comparisons. The curved bumblebee model outperforms the others due to its relatively better fitting result and AIC's smaller penalty for model complexity. However, according to Δ BIC the joint data still favor the simpler Λ CDM model. The contrasting results highlight the influence of model complexity definitions on data interpretation.

4. CONCLUSIONS AND SUMMARY

In this paper, we present Bayesian posterior probability constraints on an unconventional cosmological model based on the bumblebee gravitational theory using mul-

Table 1. Marginalized constrained data of the parameters

Model	Parameters	SNe Ia	BAO	CC	GRB	SNe Ia + BAO	SNe Ia + BAO + CC + GRB
Flat bumblebee	H_0	73.04 ± 0.26	–	68.93 ± 2.96	–	73.53 ± 0.23	73.61 ± 0.22
	$\tilde{\xi}_1$	–	0.70 ± 0.02	–	–	0.77 ± 0.02	0.75 ± 0.02
	α	-1.15 ± 0.19	-1.15 ± 0.005	-1.17 ± 0.26	-1.59 ± 0.29	-1.13 ± 0.003	-1.14 ± 0.003
Curved bumblebee	H_0	72.90 ± 0.31	–	68.48 ± 4.06	–	72.93 ± 0.24	72.96 ± 0.28
	$\tilde{\xi}_1$	–	0.82 ± 0.12	–	–	0.93 ± 0.05	0.91 ± 0.06
	α	-1.33 ± 0.35	-1.18 ± 0.03	-1.20 ± 0.42	-1.66 ± 0.40	-1.20 ± 0.02	-1.20 ± 0.02
	$\Omega_{\mathcal{K}0}$	0.29 ± 0.36	0.18 ± 0.16	-0.01 ± 0.62	–	0.29 ± 0.06	0.29 ± 0.07
Λ CDM	H_0	72.97 ± 0.26	–	67.75 ± 3.13	–	73.38 ± 0.22	73.44 ± 0.22
	$\Omega_{m,0}$	0.35 ± 0.02	0.27 ± 0.02	0.33 ± 0.06	–	0.31 ± 0.01	0.30 ± 0.01

Table 2. Comparison of Models

Model	χ^2_{\min}	red. χ^2	AIC	Δ AIC	BIC	Δ BIC
Pantheon+ SNe Ia						
Λ CDM	745.40	0.44	-1142.39	0.00	-1131.52	0.00
Flat bumblebee	745.45	0.44	-1140.33	2.06	-1124.03	7.49
Curved bumblebee	744.89	0.44	-1138.89	3.50	-1117.16	14.36
BAO						
Λ CDM	5.23	1.05	4.99	0.00	1.88	0.00
Flat bumblebee	5.38	1.35	12.14	7.16	3.98	2.10
Curved bumblebee	4.53	1.51	25.29	20.30	5.08	3.20
CC						
Λ CDM	14.60	0.44	286.48	0.00	289.21	0.00
Flat bumblebee	14.59	0.46	288.87	2.39	292.76	3.55
Curved bumblebee	14.54	0.47	291.38	4.90	296.27	7.05
GRB						
Λ CDM	174.86	1.00	200.77	0.00	216.36	0.00
Flat bumblebee	178.32	1.03	204.10	3.33	222.73	6.38
Curved bumblebee	175.83	1.02	206.15	5.38	227.92	11.56
Pantheon+ SNe Ia + BAO						
Λ CDM	760.05	0.45	-1134.99	6.00	-1124.11	0.00
Flat bumblebee	767.36	0.45	-1125.67	15.32	-1109.36	14.75
Curved bumblebee	750.03	0.44	-1140.99	0.00	-1101.91	22.19
Pantheon+ SNe Ia + BAO + CC + GRB						
Λ CDM	960.61	0.50	-642.01	3.76	-614.24	0
Flat bumblebee	965.94	0.50	-632.76	13.01	-599.44	14.80
Curved bumblebee	954.75	0.50	-645.77	0.00	-591.88	22.36

tiple cosmological probes. Our approach has incorporated emerging probes such as cosmic chronometers (CC, Section 2.3) and gamma-ray bursts (GRBs, Section 2.4) alongside well-established SNe Ia (Section 2.1) and BAO datasets (Section 2.2). The results demonstrate that the bumblebee theory provides a compatible fit to the current observational data. Furthermore, the model’s viability as an alternative to the Λ CDM framework is supported by information criteria calculations (AIC and BIC). In particular, the curved bumblebee model favors an open universe with $\Omega_{\mathcal{K}0} \sim 0.29$, challenging the traditional flat universe geometry.

We show that the constraints from the four probes are consistent within the 2σ level, and the best-fit results from the joint constraints effectively explain each individual dataset (Figure 3). By calculating the AIC and BIC for the best-fit results under different scenarios (Table 2), we find that while the bumblebee model slightly underperforms compared to Λ CDM model at the single-probe level, it does not exhibit strong disagreement. For the joint constraints, the curved bumblebee model, despite its higher complexity, achieves the best agreement with the data, with the lowest AIC among all models. This highlights the possibility of the bumblebee model as a viable modification to standard cosmology.

Interestingly, the joint constraints reveal a divergence in the conclusions drawn from AIC and BIC: AIC favors the curved bumblebee model, while BIC prefers the Λ CDM model. This discrepancy arises from the differing penalties applied to model complexity. We argue that debating the superiority of AIC versus BIC is less meaningful. Instead, we present both results to provide comprehensive insights for future research.

The development and incorporation of emerging cosmological probes offer opportunities to perform independent consistency checks on models, aiding in the assessment of whether a modified gravity theory remains viable and in achieving tighter parameter constraints. However, we must emphasize that before combining new probes for joint posterior analysis, it is critical to verify that no significant biases exist between them and established probes. Severe biases could create tension

between probes under the same model, rendering joint constraints meaningless and potentially leading to incorrect rejection of the model. Additionally, new methods should carefully evaluate potential sources of systematic error, adopting the most conservative error estimates to avoid prematurely discarding valid models.

We thank Prof. Cheng Zhao for his valuable insights. We acknowledge the Tsinghua Astrophysics High-Performance Computing platform for providing the computational and storage resources that supported this research.

Software: emcee (Foreman-Mackey et al. 2013), ChainConsumer (Hinton 2016),

REFERENCES

- Akaike, H. 1974, IEEE Transactions on Automatic Control, 19, 716, doi: [10.1109/TAC.1974.1100705](https://doi.org/10.1109/TAC.1974.1100705)
- Akrami, Y., et al. 2021, Modified Gravity and Cosmology: An Update by the CANTATA Network, ed. E. N. Saridakis, R. Lazkoz, V. Salzano, P. Vargas Moniz, S. Capozziello, J. Beltrán Jiménez, M. De Laurentis, & G. J. Olmo (Springer), doi: [10.1007/978-3-030-83715-0](https://doi.org/10.1007/978-3-030-83715-0)
- Amati, L., Frontera, F., Tavani, M., et al. 2002, A&A, 390, 81, doi: [10.1051/0004-6361:20020722](https://doi.org/10.1051/0004-6361:20020722)
- Bailey, Q. G., & Kostelecký, V. A. 2006, PhRvD, 74, 045001, doi: [10.1103/PhysRevD.74.045001](https://doi.org/10.1103/PhysRevD.74.045001)
- Bamba, K., Capozziello, S., Nojiri, S., & Odintsov, S. D. 2012, Ap&SS, 342, 155, doi: [10.1007/s10509-012-1181-8](https://doi.org/10.1007/s10509-012-1181-8)
- Bluhm, R., & Kostelecký, V. A. 2005, PhRvD, 71, 065008, doi: [10.1103/PhysRevD.71.065008](https://doi.org/10.1103/PhysRevD.71.065008)
- Brout, D., Scolnic, D., Popovic, B., et al. 2022, ApJ, 938, 110, doi: [10.3847/1538-4357/ac8e04](https://doi.org/10.3847/1538-4357/ac8e04)
- Bucher, M., & Turok, N. 1995, PhRvD, 52, 5538, doi: [10.1103/PhysRevD.52.5538](https://doi.org/10.1103/PhysRevD.52.5538)
- Copeland, E. J., Sami, M., & Tsujikawa, S. 2006, International Journal of Modern Physics D, 15, 1753, doi: [10.1142/S021827180600942X](https://doi.org/10.1142/S021827180600942X)
- DESI Collaboration, Adame, A. G., Aguilar, J., et al. 2024a, arXiv e-prints, arXiv:2404.03002, doi: [10.48550/arXiv.2404.03002](https://doi.org/10.48550/arXiv.2404.03002)
- . 2024b, arXiv e-prints, arXiv:2404.03000, doi: [10.48550/arXiv.2404.03000](https://doi.org/10.48550/arXiv.2404.03000)
- Foreman-Mackey, D., Hogg, D. W., Lang, D., & Goodman, J. 2013, PASP, 125, 306, doi: [10.1086/670067](https://doi.org/10.1086/670067)
- Hellings, R. W., & Nordtvedt, K. 1973, PhRvD, 7, 3593, doi: [10.1103/PhysRevD.7.3593](https://doi.org/10.1103/PhysRevD.7.3593)
- Hinton, S. R. 2016, The Journal of Open Source Software, 1, 00045, doi: [10.21105/joss.00045](https://doi.org/10.21105/joss.00045)
- Huang, L., Huang, Z., Luo, X., He, X., & Fang, Y. 2021, Phys. Rev. D, 103, 123521, doi: [10.1103/PhysRevD.103.123521](https://doi.org/10.1103/PhysRevD.103.123521)
- Ji, P., & Shao, L. 2024, Communications in Theoretical Physics, 76, 107401, doi: [10.1088/1572-9494/ad5aeb](https://doi.org/10.1088/1572-9494/ad5aeb)
- Kass, R. E., & Raftery, A. E. 1995, Journal of the american statistical association, 90, 773
- Kostelecký, V. A. 2004, PhRvD, 69, 105009, doi: [10.1103/PhysRevD.69.105009](https://doi.org/10.1103/PhysRevD.69.105009)
- Linde, A. 1998, PhRvD, 58, 083514, doi: [10.1103/PhysRevD.58.083514](https://doi.org/10.1103/PhysRevD.58.083514)
- Moresco, M. 2023, arXiv e-prints, arXiv:2307.09501, doi: [10.48550/arXiv.2307.09501](https://doi.org/10.48550/arXiv.2307.09501)
- Moresco, M., Pozzetti, L., Cimatti, A., et al. 2016, JCAP, 2016, 014, doi: [10.1088/1475-7516/2016/05/014](https://doi.org/10.1088/1475-7516/2016/05/014)
- Moresco, M., Amati, L., Amendola, L., et al. 2022, Living Reviews in Relativity, 25, 6, doi: [10.1007/s41114-022-00040-z](https://doi.org/10.1007/s41114-022-00040-z)
- Reichart, D. E., Lamb, D. Q., Fenimore, E. E., et al. 2001, ApJ, 552, 57, doi: [10.1086/320434](https://doi.org/10.1086/320434)
- Riess, A. G., Filippenko, A. V., Challis, P., et al. 1998, AJ, 116, 1009, doi: [10.1086/300499](https://doi.org/10.1086/300499)
- Schwarz, G. 1978, The Annals of Statistics, 6, 461, doi: [10.1214/aos/1176344136](https://doi.org/10.1214/aos/1176344136)
- Scolnic, D. M., Jones, D. O., Rest, A., et al. 2018, ApJ, 859, 101, doi: [10.3847/1538-4357/aab9bb](https://doi.org/10.3847/1538-4357/aab9bb)
- Stern, D., Jimenez, R., Verde, L., Kamionkowski, M., & Stanford, S. A. 2010, JCAP, 2010, 008, doi: [10.1088/1475-7516/2010/02/008](https://doi.org/10.1088/1475-7516/2010/02/008)

Yang, Y. 2005, *Biometrika*, 92, 937,
doi: [10.1093/biomet/92.4.937](https://doi.org/10.1093/biomet/92.4.937)